

# Area Selective Growth of Titanium Diselenide Thin Films into Micropatterned Substrates by Low-Pressure Chemical Vapor Deposition

Sophie L. Benjamin,<sup>†</sup> C. H. (Kees) de Groot,<sup>‡</sup> Chitra Gurnani,<sup>†</sup> Andrew L. Hector,<sup>†</sup> Ruomeng Huang,<sup>‡</sup> Konstantin Ignatyev,<sup>§</sup> William Levason,<sup>†</sup> Stuart J. Pearce,<sup>‡</sup> Fiona Thomas,<sup>†</sup> and Gillian Reid\*,<sup>†</sup>

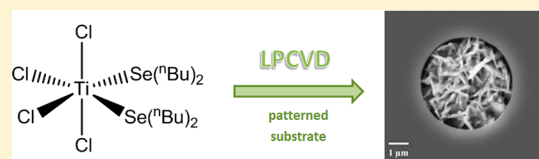
<sup>†</sup>Chemistry and <sup>‡</sup>Electronics and Computer Science, University of Southampton, Southampton, SO17 1BJ, United Kingdom

<sup>§</sup>Diamond Light Source Ltd., Didcot, OX11 0DE, United Kingdom

## Supporting Information

**ABSTRACT:** The neutral, distorted octahedral complex  $[\text{TiCl}_4(\text{Se}^n\text{Bu}_2)_2]$  (1), prepared from the reaction of  $\text{TiCl}_4$  with the neutral  $\text{Se}^n\text{Bu}_2$  in a 1:2 ratio and characterized by IR and multinuclear ( $^1\text{H}$ ,  $^{13}\text{C}\{^1\text{H}\}$ ,  $^{77}\text{Se}\{^1\text{H}\}$ ) NMR spectroscopy and microanalysis, serves as an efficient single-source precursor for low-pressure chemical vapor deposition (LPCVD) of titanium diselenide,  $\text{TiSe}_2$ , films onto  $\text{SiO}_2$  and TiN substrates. X-ray diffraction patterns on the deposited films are consistent with single-phase, hexagonal 1T- $\text{TiSe}_2$  ( $P\bar{3}m1$ ), with evidence of some preferred orientation of the crystallites in thicker films. The composition and structural morphology was confirmed by scanning electron microscopy (SEM), energy dispersive X-ray, and Raman spectroscopy. SEM imaging shows hexagonal plate crystallites growing perpendicular to the substrate, but these tend to align parallel to the surface when the quantity of reagent is reduced. The resistivity of the crystalline  $\text{TiSe}_2$  films is  $3.36 \pm 0.05 \times 10^{-3} \Omega\cdot\text{cm}$  with a carrier density of  $1 \times 10^{22} \text{ cm}^{-3}$ . Very highly selective film growth from the reagent was observed onto photolithographically patterned substrates, with film growth strongly preferred onto the conducting TiN surfaces of  $\text{SiO}_2/\text{TiN}$  patterned substrates.  $\text{TiSe}_2$  is selectively deposited within the smallest 2  $\mu\text{m}$  diameter TiN holes of the patterned TiN/ $\text{SiO}_2$  substrates. The variation in crystallite size with different diameter holes is determined by microfocus X-ray diffraction and SEM, revealing that the dimensions increase with the hole size, but that the thickness of the crystals stops increasing above  $\sim 20 \mu\text{m}$  hole size, whereas their lengths/widths continue to increase.

**KEYWORDS:** Selective deposition, single-source precursor, titanium selenide, chemical vapor deposition, selenoether, microfocus X-ray diffraction



## 1. INTRODUCTION

Many transition-metal dichalcogenides form layered structures related to that of  $\text{CdI}_2$  and these are emerging as extremely important functional materials.<sup>1</sup> Recent developments in graphene science have inspired the exploitation of the remarkable properties of layered transition-metal chalcogenides, such as strong spin splitting and access to a range of bandgaps. These materials are promising candidates for spintronics,<sup>2</sup> energy storage devices,<sup>3</sup> electrocatalysts for hydrogen evolution,<sup>4</sup> and as high-performance materials for optoelectronics.<sup>5</sup> Titanium diselenide is one of the most widely studied metal chalcogenides due to its intriguing electronic properties. In addition to semimetallic behavior, it exhibits charge density wave transitions at lower temperatures<sup>6</sup> and superconductivity with Cu intercalation.<sup>7</sup> The properties of  $\text{TiSe}_2$  can vary with the form, morphology, and thickness of the films; for example, recently prepared one-dimensional chains in the hybrid organic phase  $\text{TiSe}_2(\text{en})$  ( $\text{en} = 1,2\text{-diaminoethane}$ ) have a direct bandgap of 1.21 eV compared to the bulk phase, which has a 0.2 eV overlap between the conduction and valence bands.<sup>8</sup> By sintering pellets of  $\text{TiSe}_2$  under Ar, it is possible to produce nanotube and nanowire forms.<sup>9</sup> Hence, the ability to control

the size, dimensionality, and morphology could offer an entry into new behavior and applications of chalcogenide materials.

We have recently shown that highly selective growth of crystalline single-phase  $\text{SnSe}_2$  films within photolithographically patterned substrates can be achieved via single-source reagents  $[\text{SnCl}_4(\text{BuSe}(\text{CH}_2)_n\text{Se}^n\text{Bu})]$  ( $n = 2$  or 3).<sup>10</sup> Selective growth specifically within small conductive TiN features on the micrometer/submicrometer diameter is a very attractive prospect for a number of applications in the electronic industry, including phase change memory materials and thermoelectric materials.

Previous chemical vapor deposition (CVD)-based approaches to the deposition of metal chalcogenide films have included both single- and dual-source atmospheric pressure CVD. The latter used volatile  $\text{MCl}_x$  with a range of thiols, thiolates, or dialkyl diselenides, or aerosol-assisted CVD using  $\text{M}(\text{NMe}_2)_x$  and  $\text{RSH}$  or  $\text{Bu}_2\text{S}$ .<sup>11</sup> We have used group 4 metal bis-cyclopentadienyl complexes with selenolate ligands as

**Received:** July 19, 2013

**Revised:** September 20, 2013

**Published:** November 5, 2013

single-source precursors for CVD of  $\text{MSe}_2$  films ( $\text{M} = \text{Ti}$ ,  $\text{Zr}$ , and  $\text{Hf}$ )<sup>12</sup> and the *o*-xylyl-based chalcogenoether complexes  $[\text{TiCl}_4\{\text{o-C}_6\text{H}_4(\text{CH}_2\text{EMe})_2\}]$  as reagents to deposit  $\text{TiE}_2$  ( $\text{E} = \text{S}$  or  $\text{Se}$ ).<sup>13</sup> Winter and co-workers<sup>14</sup> previously used  $[\text{TiCl}_4(\text{SeEt}_2)_2]$  (2) for production of  $\text{TiSe}_2$  thin films, but these were reported to be unstable in air, degrading to give amorphous titanium oxy-selenide materials.

Here we report the low-pressure chemical vapor deposition (LPCVD) of single-phase, crystalline  $\text{TiSe}_2$  thin films onto  $\text{SiO}_2$  and  $\text{TiN}$  substrates using the molecular single-source precursor  $[\text{TiCl}_4(\text{Se}^n\text{Bu}_2)_2]$  (1). This work demonstrates that the approach, specifically using selenoether complexes as single-source precursors to achieve very highly selective film growth, is also relevant to the transition-metal chalcogenides. Moreover, we show that the scale of the patterning directly influences the morphology of the deposit, and we describe the use of synchrotron-based microfocus X-ray diffraction, together with scanning electron microscopy, to probe the morphology of the materials deposited as a function of template hole size, down to features of dimensions  $2 \mu\text{m}$  diameter  $\times 1 \mu\text{m}$  deep.

## 2. EXPERIMENTAL SECTION

**2.1. Precursor Preparation and Characterization.** All reactions were conducted using Schlenk, vacuum line, and glove box techniques under a dry nitrogen atmosphere. The reagents were manipulated using a glove box. Dichloromethane was dried over  $\text{CaH}_2$ .  $^n\text{BuLi}$  was obtained from Aldrich and used as-received.  $^n\text{Bu}_2\text{Se}$ <sup>15</sup> and  $[\text{TiCl}_4(\text{SeEt}_2)_2]$  (2)<sup>14</sup> were prepared according to literature methods. Infrared spectra were recorded as neat thin films (unless otherwise stated) between  $\text{CsI}$  plates using a Perkin-Elmer Spectrum100 spectrometer over the range  $4000\text{--}200 \text{ cm}^{-1}$ .  $^1\text{H}$  and  $^{13}\text{C}\{\text{H}\}$  NMR spectra were recorded in  $\text{CDCl}_3$  or  $\text{CD}_2\text{Cl}_2$ , using a Bruker AV300 spectrometer.  $^{77}\text{Se}\{\text{H}\}$  NMR spectra were recorded using a Bruker DPX400 spectrometer and are referenced to neat  $\text{Me}_2\text{Se}$ . Electrospray (ES) MS data were obtained from solutions in  $\text{MeCN}$  using a VG Biotech Platform. Thermogravimetric analyses (TGA) used a Mettler Toledo TGA/SDTA851e analyzer under a flow of Ar at  $65 \text{ mL/min}$ , contained within a dry,  $\text{N}_2$ -purged glove box. The temperature was increased at a rate of  $10^\circ\text{C}/\text{min}$ . Microanalytical data were obtained from Medac Ltd.

$[\text{TiCl}_4(^n\text{Bu}_2\text{Se})_2]$  (1):  $^n\text{Bu}_2\text{Se}$  (0.386 g, 2.0 mmol) was dissolved in  $\text{CH}_2\text{Cl}_2$  (5 mL) and added to a solution of  $\text{TiCl}_4$  (0.188 g, 1.0 mmol) in rigorously anhydrous  $\text{CH}_2\text{Cl}_2$  (10 mL). The solution was stirred constantly in an ice bath. A red solution was formed immediately and further stirred for 1 h. The volatile components were removed in *vacuo* to give a dark red oil. Yield: 0.53 g, 82%. IR (neat thin film):  $\nu/\text{cm}^{-1} = 354$  (sh), 395 (vs), 430 (sh) ( $\text{Ti}-\text{Cl}$ ).  $^1\text{H}$  NMR ( $\text{CDCl}_3$ , 295 K):  $\delta = 0.96$  (t) [3H]  $\text{Me}$ , 1.47 (m) [2H]  $\text{CH}_2$ , 1.78 (m) [2H]  $\text{CH}_2$ , 3.00 (br) [2H]  $\text{CH}_2\text{Se}$ .  $^{13}\text{C}\{\text{H}\}$  ( $\text{CDCl}_3$ , 295 K):  $\delta = 13.52$ , 22.86, 31.70, 35.13.  $^{77}\text{Se}\{\text{H}\}$  NMR ( $\text{CH}_2\text{Cl}_2/\text{CD}_2\text{Cl}_2$ , 298 K):  $\delta = 310$ . Anal. Calcd for  $\text{C}_{16}\text{H}_{36}\text{Cl}_4\text{Se}_2\text{Ti}$ : C, 33.4; H, 6.3. Found: C, 33.3; H, 6.5%.

**2.2. Substrate Preparation.** Substrates were prepared as described in ref 10.

**2.3. LPCVD onto  $\text{SiO}_2$  or  $\text{TiN}$  Substrates.** In a typical experiment, ca. 120 mg of the reagent and the substrates ( $\sim 1 \times 5 \times 25 \text{ mm}$ ) were loaded into a closed-end silica tube in a glove box. The substrates were positioned end-to-end through the heated zone. The tube was set in the furnace such that the precursor was (ca. 2 cm) away from the edge of the heated zone. The tube was evacuated to  $0.5 \text{ mmHg}$ , and the furnace was set to  $873 \text{ K}$  (the temperature in the hot zone was measured as  $858 \text{ K}$ ). After ca. 20 min the tube position was adjusted to move the precursor further toward the hot zone (ca. 1 cm away from edge of the heated zone) until the oil gradually began to evaporate. At this point the sample position was maintained until the entire precursor had evaporated, leaving behind no residue. The tube was then cooled to room temperature and transferred to the glove box where the tiles were removed and stored for further characterization.

The LPCVD experiments using precursor (1) produced purple matt powdery films of  $\text{TiSe}_2$ , with dense coverage on tiles in the hottest zone where the temperature was about  $845\text{--}858 \text{ K}$ . No significant differences were observed in the film morphology across the tiles. Samples were not strongly adhered to the tiles. The thicker films appeared to be relatively air-stable. In contrast, using  $\sim 5\text{--}10 \text{ mg}$  of precursor resulted in very thin films which were purple and reflective in appearance; these tended to be much more sensitive to moist air. However, upon careful handling within the glove box, good quality  $\text{TiSe}_2$  films could be retained without degradation for several weeks. Excellent reproducibility and similar characterization data were obtained from several different samples.

**2.4. Film Characterization.** XRD patterns were collected in grazing incidence ( $\theta_1 = 3^\circ$ ) using a Bruker D8 with GADDS diffractometer ( $\text{Cu}-\text{K}\alpha_1$ ) for phase identification purposes. To examine preferred orientation, a Rigaku SmartLab system with a 2-bounce primary monochromator ( $\text{Cu}-\text{K}\alpha_1$ ) was used in symmetric  $\theta\text{-}2\theta$  geometry and the data refined against a standard literature  $\text{TiSe}_2$  model<sup>16</sup> using the GSAS package.<sup>17</sup> The March-Dollase preferred orientation ratio was used to model crystallite orientation relative to the substrate normal. Microfocus XRD patterns were collected at beamline I18 of the Diamond Light Source using  $16.8 \text{ keV}$  ( $0.738 \text{ \AA}$ ) X-rays focused to a  $2 \times 4 \mu\text{m}$  FWHM spot. An aligned optical microscope was used to locate regions of interest on the sample and diffraction patterns were collected through the  $0.6 \text{ mm}$  Si substrate and  $125 \text{ nm}$   $\text{TiN}$  film using a  $4000 \times 2500$  pixel CCD detector; a data collection on an identical substrate with no deposited film was used to subtract the substrate contributions to the signal.

Raman scattering spectra of the deposited films were measured at room temperature on a Renishaw InVia Micro Raman Spectrometer using a helium–neon laser with a wavelength of  $532 \text{ nm}$ . The incident laser power was adjusted to  $\sim 1 \text{ mW}$  for all samples. Scanning electron microscopy (SEM) was performed on samples at an accelerating voltage of  $10 \text{ kV}$  using a Zeiss EVO LS 25, and energy dispersive X-ray (EDX) data were obtained with an Oxford INCA x.act X-ray detector. The cross-section SEM measurements were carried out with a field emission SEM (Jeol JSM 7500F) at an accelerating voltage of  $2 \text{ kV}$ . Hall measurements were performed at room temperature on a Nanometrics HL5500PC with a current of  $1 \text{ mA}$ .

**2.5. LPCVD onto Patterned  $\text{TiN/SiO}_2$  Substrates.**  $\text{TiN/SiO}_2$  patterned substrates ( $1 \times 5 \times 25 \text{ mm}$ ) were loaded with  $5\text{--}8 \text{ mg}$  of reagent into a closed-end silica tube in a glove box as described above, and depositions were performed similarly over ca. 40 min.

## 3. RESULTS AND DISCUSSION

We have previously described the synthesis, properties, and structures of thio- and selenoether complexes of  $\text{TiX}_4$ . These are distorted *cis*-octahedral complexes of the form  $[\text{TiX}_4(\text{L-L})]$ , where L-L is  $\text{MeE}(\text{CH}_2)_n\text{EMe}$  ( $\text{E} = \text{S}$ ,  $\text{Se}$ ;  $n = 2$  or 3), *o*- $\text{C}_6\text{H}_4(\text{CH}_2\text{EMe})_2$ , and *o*- $\text{C}_6\text{H}_4(\text{EMe})_2$ .<sup>13</sup> All of these complexes are hydrolytically sensitive, forming oxo-bridged dinuclear species upon partial hydrolysis. The  $[\text{TiCl}_4(\text{SeEt}_2)_2]$  (2),<sup>14</sup> *o*-xylyl-diselenoether, and *o*-xylyl-dithioether complexes of titanium(IV) chloride were tested as reagents for low-pressure CVD, yielding  $\text{TiSe}_2$  and  $\text{TiS}_2$ , respectively. The sulfide remains a very rare example of metal sulfide film growth via a single-source metal-thioether complex.<sup>13</sup>

**3.1. Reagent Preparation and Characterization.** The moisture-sensitive  $[\text{TiCl}_4(\text{Se}^n\text{Bu}_2)_2]$  (1) was synthesized and isolated in good yield as a dark red oil by direct reaction of  $\text{TiCl}_4$  and ligand in anhydrous  $\text{CH}_2\text{Cl}_2$ . The compound showed no degradation over several weeks if stored under  $\text{N}_2$  in the freezer. Samples were manipulated in an  $\text{N}_2$  purged, dry ( $<1 \text{ ppm H}_2\text{O}$ ) glove box and was characterized by IR,  $^1\text{H}$ ,  $^{13}\text{C}\{\text{H}\}$ , and  $^{77}\text{Se}\{\text{H}\}$  NMR spectroscopy, with the data in very good agreement with related complexes, and consistent with a distorted *cis*-octahedral coordination environment.<sup>13</sup> The

*n*-butyl substituents were introduced in the ligand with the aim of providing an easy thermal decomposition pathway via  $\beta$ -hydride elimination, for the reagent during the CVD experiments. A similar *cis*-octahedral moiety is present in  $[\text{TiCl}_4(\text{SeEt}_2)_2]$  (2),<sup>14</sup> which was obtained and characterized similarly.

TGA measurements on (1) and (2) (ESI) show the onset of evaporation at  $\sim 380$  and  $360$  K, respectively, with mass loss occurring in a single step for (1), leaving a residue (8.5%) which is unaffected above  $\sim 570$  K. For (2), mass loss occurs in three steps, with loss of  $\sim 67\%$  between  $360$  and  $430$  K, followed by further mass losses of  $\sim 18\%$  between  $430$  and  $480$  K and 8% between  $480$  and  $560$  K, with a small amount of residue ( $\sim 11\%$ ) remaining at higher temperatures. In both cases the residue is significantly less than that expected for decomposition to  $\text{TiSe}_2$  (35.7% and 44.4%, respectively, for (1) and (2)); hence, it appears that the TGA data show evaporation of the precursor as the dominant thermal process under 1 atm pressure of inert gas.

LPCVD experiments using (1) were performed using freshly prepared samples, as the reagent tended to darken over a few days to weeks if maintained at room temperature in the glove box, indicative of decomposition.

**3.2. Thin Film Growth and Analysis.** LPCVD of complex (1) was undertaken with the furnace temperature set at  $873$  K, leading to complete evaporation of the precursor compound and deposition of intensely purple matt films onto the  $\text{SiO}_2$  substrate. Similar behavior was also observed on the TiN substrate. Reducing the temperature to  $773$  or  $823$  K resulted in poorer coverage and incomplete decomposition of the precursor; hence, the deposition temperature of  $873$  K was selected (this was also the temperature previously used for LPCVD experiments on (2)).<sup>14</sup> Initially, depositions used ca.  $50$ – $100$  mg of precursor and SEM analysis on these  $\text{TiSe}_2$  films showed a regular morphology formed of hexagonal plate crystallites. Most of the crystallites are aligned with their flat surfaces perpendicular to the substrate surface (Figure 1a,b) and cross-sectional SEM showed these films were  $4$ – $5 \mu\text{m}$

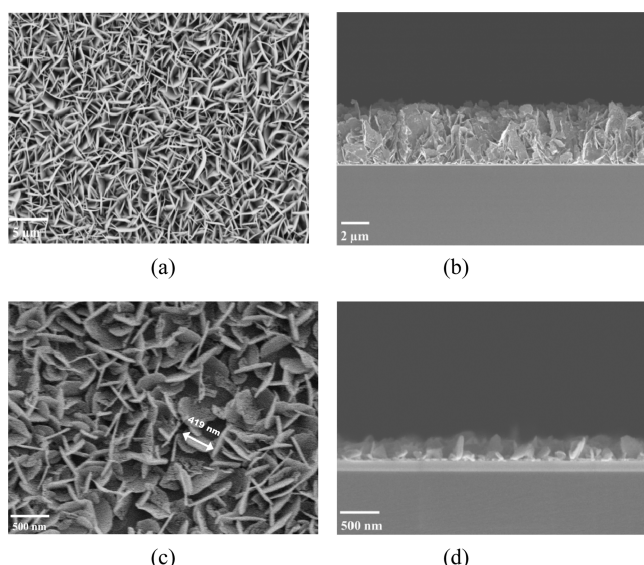


**Figure 1.** SEM images of hexagonal  $\text{TiSe}_2$ : (a) top view and (b) cross section of film deposited from  $100$  mg of reagent, showing the film thickness of  $\sim 4 \mu\text{m}$ ; (c) top view of a much thinner  $\text{SnSe}_2$  film deposited using  $5$  mg of reagent; (d) cross section of this thin film.

thick. However, cross-section SEM analysis of reagent-limited films grown at  $873$  K using  $5$ – $7$  mg of precursor (1) showed films that were much thinner (ca.  $300$  nm) (Figure 1c,d).

LPCVD experiments using precursor (2), which is a solid at ambient temperatures, were in accord with those reported by Winter and co-workers,<sup>14</sup> and although visually the two reagents appear to behave quite similarly, in our hands precursor (2) tended to give much thinner films of  $\text{TiSe}_2$ . Subsequent work therefore focused on (1).

XRD measurements on the material deposited from (1) confirmed it as crystalline hexagonal  $\text{TiSe}_2$  in all cases, with strongly textured diffraction patterns as expected from the large, oriented crystallites observed in the SEM images. No crystalline impurities were observed. Rietveld refinement of a pattern from a thick film collected in symmetric  $\theta$ – $2\theta$  geometry (Figure 2)

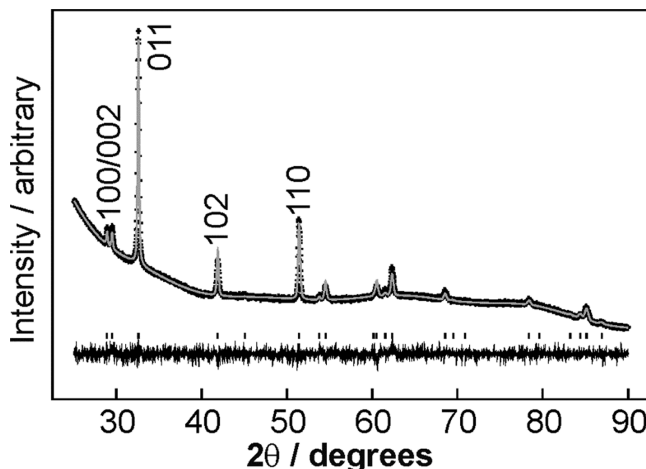


**Figure 2.** Fit to the XRD pattern for  $\text{TiSe}_2$  in  $P\bar{3}m1$  ( $R_{wp} = 1.7\%$ ,  $R_p = 1.2\%$ ). Crosses mark the data points, the upper continuous line the fit, and the lower continuous line the difference. Tick marks show the positions of allowed reflections, the first five of which are also labeled. The background shape is due to the amorphous silica substrate.

revealed lattice parameters of  $a = 3.53489(14) \text{ \AA}$  and  $c = 6.0036(4) \text{ \AA}$ , close to those of bulk  $\text{TiSe}_2$  (space group  $P\bar{3}m1$ ,  $a = 3.540(1) \text{ \AA}$  and  $c = 6.008(3) \text{ \AA}$ ).<sup>16</sup> As expected from the crystallite orientations observed by SEM, the data show a clear suppression of the intensity of reflections strongly associated with the  $c$ -axis; this was modeled via a preferred orientation fraction of  $0.605(2)$  in the  $110$  direction.

The EDX measurements show that the Ti:Se ratio is 1:2 (29.2% Ti, 59.2% Se), and while there is no residual Cl impurity present, a small amount of carbon (7.0%) incorporation is observed, most likely as residual contamination on the surface of the crystallites derived from the butyl substituents in the precursor (Si and O from the silica substrate account for the remaining 5%). Raman spectra were recorded on several samples and showed an intense peak at  $197 \text{ cm}^{-1}$  and a weaker peak at  $138 \text{ cm}^{-1}$  (Figure 3) corresponding to Raman active  $A_{1g}$  and  $E_g$  symmetry phonons of the bulk hexagonal 1T- $\text{TiSe}_2$ , respectively.<sup>18</sup> Measurements taken at several regions on the sample showed no significant variation in peak width or relative intensities. Other peaks corresponding to secondary phases such as  $\text{TiO}_2$  were not evident.

**3.3. Hall Measurements.** Conductivity values were obtained by Hall effect measurements.  $\text{TiSe}_2$  thin films were deposited on a sputtered  $\text{SiO}_2$  film to insulate the substrate.

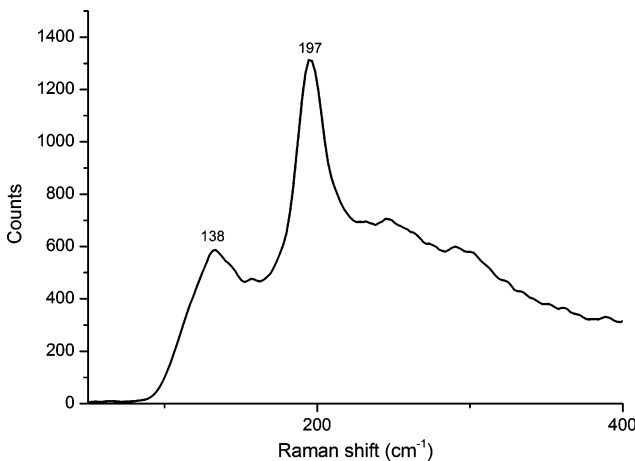


**Figure 3.** Raman spectrum of TiSe<sub>2</sub> thin film grown by LPCVD at 873 K from (1) showing the A<sub>1g</sub> and E<sub>g</sub> modes. The broad features to high frequency are from the substrate.

Films with thicknesses of 3.5 μm were used for the measurements. The experiments were conducted under a magnetic field of 0.5 T at 300 K.

The resistivity of the TiSe<sub>2</sub> films was found to be (3.36 ± 0.05) × 10<sup>-3</sup> Ω·cm. Similar values have been reported in literature<sup>19,20</sup> and this high conductivity is consistent with the very small bandgap for TiSe<sub>2</sub> of around 150 meV.<sup>21</sup> This small bandgap results in a near intrinsic semiconductor with both electrons and holes contributing to the conductivity and Hall coefficient<sup>22</sup> as given in

$$R_H = \frac{p\mu_h^2 - n\mu_e^2}{e(p\mu_h + n\mu_e)^2} \quad (1)$$

The Hall coefficient is -(9 ± 2) × 10<sup>-4</sup> cm<sup>3</sup>/C, hence a minimum electron carrier density of 1 × 10<sup>22</sup> cm<sup>-3</sup>. The sign of the Hall coefficient might indicate n-type conduction, but is more likely to reflect the higher electron than hole mobility.

**3.4. Selective Deposition.** Deposition experiments were performed under the same conditions onto SiO<sub>2</sub> and TiN substrates. No variations in the morphology occurred on different substrate types. Reagent-limited LPCVD experiments using 5–7 mg of precursor were undertaken onto photolithographically patterned SiO<sub>2</sub>/TiN substrates. This resulted in very highly selective deposition within the conducting TiN holes of the patterned substrates (Figure 4). The coverage was densest on the substrates which lay in the hotter zone of the furnace. This high substrate selectivity was observed for all sizes of holes

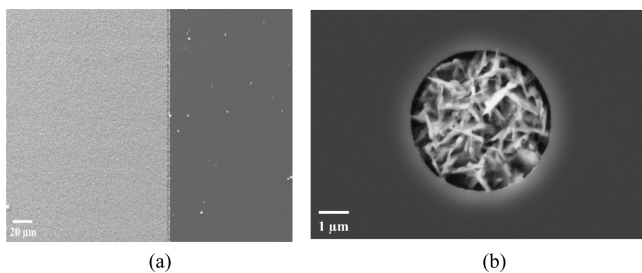


**Figure 4.** SEM images: (a) showing selective growth of TiSe<sub>2</sub> onto the TiN on a patterned TiN (left)/SiO<sub>2</sub> (right) substrate; (b) showing selective deposition of TiSe<sub>2</sub> within 5 μm TiN hole of a TiN/SiO<sub>2</sub> patterned substrate.

varying from the large (80–100 μm) diameters to the smaller (2–5 μm) diameters, as illustrated in the Figures 5 and 6, respectively.

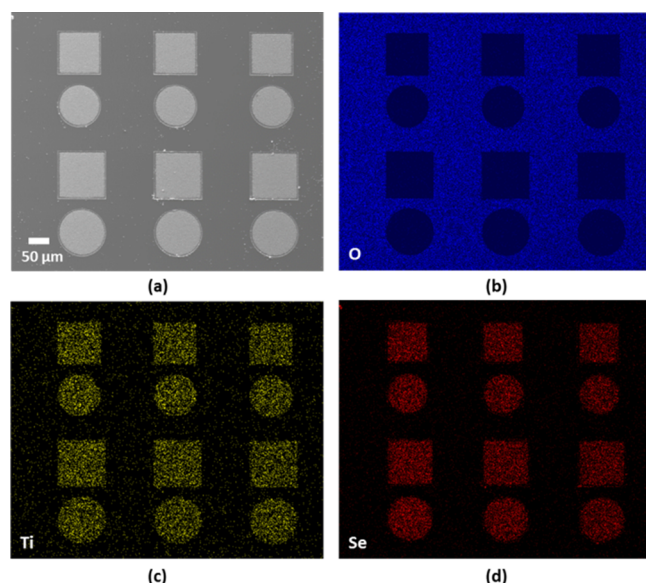


**Figure 5.** SEM image (a) and EDX element maps (b)–(d) confirming the selective deposition of TiSe<sub>2</sub> occurring only within the holes (80 μm diameter) with growth occurring preferentially onto the TiN surface. All are on the same scale shown on the first image.

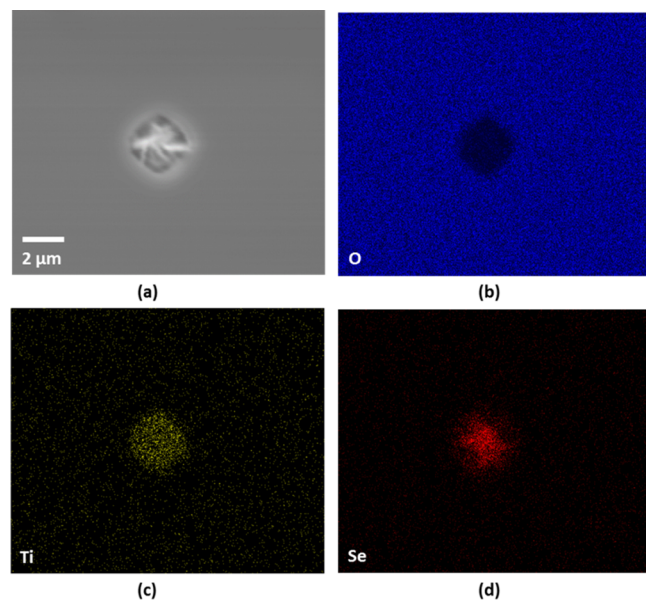


**Figure 6.** SEM image (a) and EDX element maps (b)–(d) confirming the selective deposition of TiSe<sub>2</sub> occurring only within the holes (2 μm diameter) with growth occurring preferentially onto the TiN surface. All are on the same scale shown on the first image.

Substrate selective deposition of TiSe<sub>2</sub> into 2 μm diameter holes is successful on a smaller scale than observed for SnSe<sub>2</sub> where this scale of selectivity was limited (to 5 μm) by the size of the individual SnSe<sub>2</sub> crystallites (~1.6 × 2.0 μm across the hexagon).<sup>10</sup> The SEM images suggest that the average size (in x–y plane) of individual TiSe<sub>2</sub> crystallites varies from ~1.2 μm (within 100 μm TiN holes) to ~600 nm (within 2 μm TiN holes).

Microfocus X-ray diffraction experiments were performed at beamline I18 of the Diamond Light Source using a  $2 \times 4 \mu\text{m}$  beam impinging on the region of sample of interest normal to the substrate and with the diffracted beam collected after passing through the substrate. Figure 7 shows typical diffraction

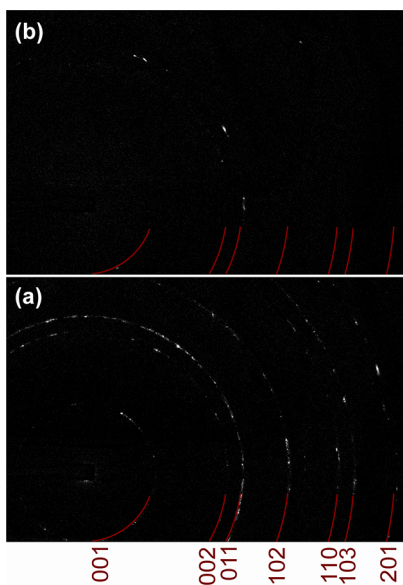


**Figure 7.** Microfocus X-ray diffraction patterns collected on  $\text{TiSe}_2$  samples selectively deposited into  $100 \mu\text{m}$  (a) and  $5 \mu\text{m}$  (b) holes.

patterns after subtraction of a background collected on a blank substrate. These patterns show conclusively that the same material was being produced in all hole sizes as on flat substrates. The beam size was small enough for the sampling region to be the same with these differently sized holes and a grid of sample positions was collected to ensure that patterns were obtained with the beam in the center of the hole, but it was found that the patterns collected from samples deposited into smaller holes were always much more heavily textured than from those deposited in larger holes. This suggests a smaller number of crystallites in the beam footprint in smaller holes, which could be related to a smaller amount of deposit, or to

larger crystallites. Examination of the crystallite sizes in SEM images (Figure 8) showed that both the length and thickness of crystallites increases with the hole size but that the thickness of the crystals stops increasing above  $\sim 20 \mu\text{m}$  hole size, whereas their lengths continue to increase.

The smallest holes have a diameter of  $2 \mu\text{m}$  and a depth determined by the  $1 \mu\text{m}$  thickness of the silica film. Combining the diffraction and SEM results shows that a smaller number of crystallites is deposited per unit area in the smaller holes and that the crystallite size is also smaller. The obvious explanations are that diffusion to the surface is less efficient than in the larger holes or that the smaller deposition area acts less efficiently to supply adsorbed species to the growth process. Neither is compelling since, with no carrier gas, the boundary layer for diffusion should be very thin and the aspect ratio of the smallest holes is not large, whereas a larger area may contain more adsorbed material, but it also has a larger area across which growth can occur. It may be that the hydrophilic side walls of the holes have a more significant effect on the transport of the precursor as the hole size becomes smaller, and that this is the determining factor controlling growth into the holes.

The high selectivity of  $\text{TiSe}_2$  onto the TiN regions using patterned  $\text{SiO}_2/\text{TiN}$  substrates can be attributed to variation in the nature of the surfaces. We have recently correlated the selective deposition with the wetting property of the substrate surface.<sup>10</sup> Cao and co-workers have very recently demonstrated a strong mediation effect of substrates for growth of layered chalcogenide materials signifying dynamics of growth reaction which leads to facile migration of metal chalcogenide adatoms onto substrates.<sup>23</sup> This very high selectivity for film deposition from the single-source selenoether ligand complexes onto the highly conducting TiN is attractive for potential applications of chalcogenide materials in electronic devices.

#### 4. CONCLUSIONS AND OUTLOOK

The molecular complex of titanium(IV) chloride with di-*n*-butyl selenide, (1), has been shown to function as an efficient single-source precursor for the low-pressure CVD of single-phase, crystalline  $\text{TiSe}_2$ , apparently superior to the more hydrolytically sensitive diethyl selenide analog, (2), reported previously.<sup>14</sup> Reagent (1) provides strong evidence for selective

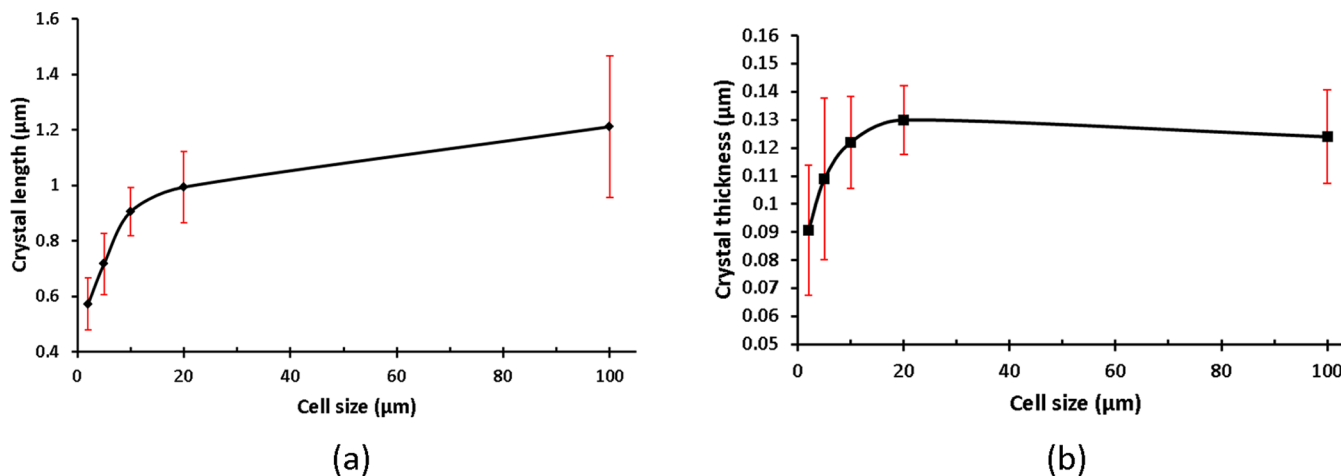


**Figure 8.** Variation of crystallite length (along *a*-axis of hexagonal plate) (a) and width (along *c*-axis) (b) with the size of hole into which the sample is deposited. The black line is to provide a guide to the eye and the values/error bars were obtained by SEM measurement of 10 crystallites in a sample.

deposition of TiSe<sub>2</sub> within photolithographically micropatterned templates via CVD, and importantly, establishes that the high substrate selectivity previously observed for SnSe<sub>2</sub> is not unique to that system, but may be a much more common phenomenon of metal chalcogenide CVD using single-source precursors derived from metal halide complexes with suitable chalcogenoether ligands. Precursor (1) forms smaller crystallites than observed for SnSe<sub>2</sub>, and allows filling of the (smallest) 2 μm diameter holes with the desired TiSe<sub>2</sub> stoichiometry. Microfocus XRD experiments show that the crystallite sizes increase with increased template hole size.

## ■ ASSOCIATED CONTENT

### Supporting Information

TGA plots for (1) and (2) (Figures S1 and S2). This material is available free of charge via the Internet at <http://pubs.acs.org>.

## ■ AUTHOR INFORMATION

### Corresponding Author

\*E-mail: g.reid@soton.ac.uk.

### Notes

The authors declare no competing financial interest.

## ■ ACKNOWLEDGMENTS

The authors thank the EPSRC (EP/I010890/1) for funding and for a Doctoral Prize (S.L.B.), the Royal Society for a Newton International Fellowship (C.G.), and Diamond Light Source for beam time under allocation SP8211-1. We also thank Dr. M. Jura and the Materials Characterization Laboratory at ISIS for access to the Rigaku SmartLab diffractometer.

## ■ REFERENCES

- (1) Chhowalla, M.; Shin, H. S.; Eda, G.; Li, L.-J.; Loh, K. P.; Zhang, H. *Nature Chem.* **2013**, *5*, 263.
- (2) Zeng, H.; Dai, J.; Yao, W.; Xiao, D.; Cui, X. *Nature Nano.* **2012**, *7*, 490.
- (3) Liu, J.; Liu, X.-W. *Adv. Mater.* **2012**, *24*, 4097.
- (4) Xiang, Q.; Yu, J.; Jaroniec, M. *J. Am. Chem. Soc.* **2012**, *134*, 6575.
- (5) Pu, J.; Yomogida, Y.; Liu, K.-K.; Li, L.-J.; Iwasa, Y.; Takenobu, T. *Nano Lett.* **2012**, *12*, 4013.
- (6) Rasch, J. C. E.; Stemmler, T.; Müller, B.; Dudy, L.; Manzke, R. *Phys. Rev. Lett.* **2008**, *101*, 237602.
- (7) Morosan, E.; Zandbergen, H. W.; Dennis, B. S.; Bos, J. W. G.; Onose, Y.; Klimczuk, T.; Ramirez, A. P.; Ong, N. P.; Cava, R. J. *Nature Phys.* **2006**, *2*, 544.
- (8) Li, T.; Liu, Y.-H.; Porter, S.; Goldberger, J. E. *Chem. Mater.* **2013**, *25*, 1477.
- (9) Chen, J.; Tao, Z.-L.; Li, S.-L.; Fan, X.-B.; Chou, S.-L. *Adv. Mater.* **2003**, *15*, 1379.
- (10) de Groot, C. H.; Gurnani, C.; Hector, A. L.; Huang, R.; Jura, M.; Levason, W.; Reid, G. *Chem. Mater.* **2012**, *24*, 4442.
- (11) (a) Boscher, N. D.; Carmalt, C. J.; Parkin, I. P. *Chem. Vap. Deposition* **2006**, *12*, 54. (b) Boscher, N. D.; Blackman, C. S.; Carmalt, C. J.; Parkin, I. P.; Prieto, A. G. *Appl. Surf. Sci.* **2007**, *253*, 6041. (c) Boscher, N. D.; Carmalt, C. J.; Parkin, I. P. *Eur. J. Inorg. Chem.* **2006**, *1255*. (d) Carmalt, C. J.; Parkin, I. P.; Peters, E. S. *Polyhedron* **2003**, *22*, 1263. (e) Peters, E. S.; Carmalt, C. J.; Parkin, I. P.; Tocher, D. A. *Eur. J. Inorg. Chem.* **2005**, 4179.
- (12) Hector, A. L.; Levason, W.; Reid, G.; Reid, S. D.; Webster, M. *Chem. Mater.* **2008**, *20*, 5100.
- (13) Reid, S. D.; Hector, A. L.; Levason, W.; Reid, G.; Waller, B. J.; Webster, M. *Dalton Trans.* **2007**, 4769.
- (14) McKarns, P. J.; Lewkebandara, T. S.; Yap, G. P. A.; Liable-Sands, L. M.; Rheingold, A. L.; Winter, C. H. *Inorg. Chem.* **1998**, *37*, 418.

- (15) Gulliver, D. J.; Hope, E. G.; Levason, W.; Murray, S. G.; Potter, D. M.; Marshall, G. L. *Chem. Soc., Perkin Trans. 2* **1984**, 429.
- (16) Riekel, C. *J. Solid State Chem.* **1976**, *17*, 389.
- (17) (a) Larson, A. C.; von Dreele, R. B. *General Structure Analysis System (GSAS)*; Los Alamos National Laboratory Report LAUR 86-748; Los Alamos National Laboratory: Los Alamos, NM, 2000. (b) Toby, B. H. *J. Appl. Crystallogr.* **2001**, *34*, 210.
- (18) (a) Holy, J. A.; Woo, K. C.; Klein, M. V.; Brown, F. C. *Phys. Rev. B* **1977**, *16*, 3628. (b) Jaswal, S. S. *Phys. Rev. B* **1979**, *20*, 5297.
- (19) May, M. M.; Brabetz, C.; Janowitz, C.; Manzke, R. *Phys. Rev. Lett.* **2011**, *107*, 176405.
- (20) Friend, R. H.; Jerome, D.; Yoffe, A. D. *J. Phys. C: Solid State Phys.* **1982**, *15*, 2183.
- (21) Rasch, J. C. E.; Stemmler, T.; Müller, B.; Dudy, L.; Manzke, R. *Phys. Rev. Lett.* **2008**, *101*, 237602.
- (22) Di Salvo, F. J.; Waszczak, J. V. *Phys. Rev. B* **1978**, *17*, 3801.
- (23) Huang, L.; Yu, Y.; Li, C.; Cao, L. *J. Phys. Chem. C* **2013**, *117*, 6469.